The 2009 IEEE/RSJ International Conference on
Intelligent Robots and Systems
October 11-15, 2009 St. Louis, USA

Effects of Swing-leg Retraction and Mass Distribution on Energy-loss Coefficient in Limit Cycle Walking

Fumihiko Asano

Abstract— **Limit cycle walkers utilizing their natural dynamics can achieve energy-efficient dynamic walking. Their heel-strike collision with the ground is generally modeled as an inelastic collision, and the discrete walking dynamics can be specified in the same manner as a rimless wheel by using the energy-loss coefficient and restored mechanical energy. Energy-loss coefficient is especially significant because it controls the gait efficiency and stability, but the value varies significantly according to the swing-leg retraction just prior to impact and robot's mass-distribution. This paper then mathematically investigates how energy-loss coefficient changes with respect to them, and discusses the effect on the gait efficiency and stability.**

I. INTRODUCTION

Limit cycle walking utilizing the robot's own natural dynamics is an approach to efficient legged locomotion. McGeer's passive dynamic walking (PDW) is a good example for efficient biped locomotion [1], and several gait generation methods inspired by PDW have been proposed. Virtual passive dynamic walking [2] and parametrically excited walking [3] are major approaches the authors proposed. The generated bipedal gait of limit cycle walkers consists of single-support and double-support phases. In general, dynamic walkers must restore mechanical energy during single-support phases to generate stable gaits because the energy-loss is caused by leg-exchange modeled as an inelastic collision. Generating energy-efficient gait rests on how to restore the lost mechanical energy effectively.

Impact dynamics also has great influences on the efficiency and stability of limit cycle walking. Energy-loss coefficient defined as a ratio of kinetic energy just after impact to that just before impact is a useful quantity to specify the property of discrete walking dynamics. The value is, however, determined by many components of the walking system such as the mass balance, joint angles at impact and angular velocities just before impact. Swing-leg retraction (SLR) is a phenomenon that the swing-leg moves backward just prior to impact [4], and has a great influence on the gait efficiency and limit cycle stability.

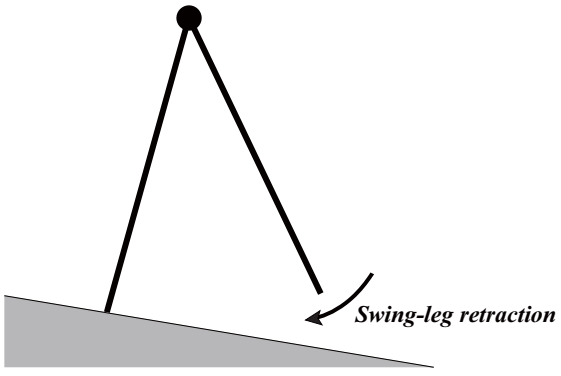

Fig. 1. Passive-dynamic walkers often exhibits swing-leg retraction just prior to impact.

F. Asano is with the School of Information Science, Japan Advanced Institute of Science and Technology, 923-1292 Ishikawa, Japan fasano@jaist.ac.jp

The authors clarified that the leg mass strongly affects the energy-loss coefficient [5]. In the simplest walking model [6], which is a compass-like biped model whose leg mass can be neglected, the energy-loss coefficient does not depend on the swing-leg dynamics and depend only on the relative hip angle at impact. This is the special case and does not hold in general models. The authors also clarified that falling down as a 1-d.o.f. rigid body dramatically extends the stable domain. A compass-like biped can achieve this only by constraining the hip joint, and this condition was termed as the quasi-constraint on impact posture [7]. On the other hand, Hobbelen and Wisse termed this condition as the zero swing-leg retraction (ZSLR) [8]. They analyzed the effect of SLR on the gait stability using the gait sensitivity norm, and showed that a gentle SLR improves the gait stability [8][9]. In these works, the importance of SLR in dynamic walking has been discussed.

Based on the observations, in this paper we mathematically analyze the effects of SLR and mass distribution on limit cycle walking from the energy-loss coefficient view-point. We first formulate the energy-loss coefficient mathematically taking SLR into account as a function of four parameters; the half inter-leg angle, the location of center of mass, the mass ratio and the ratio of angular velocities. We numerically and analytically investigate how these parameters affect the value of energy-loss coefficient. Furthermore, we discuss the relation between the energy-loss coefficient and the eigenvalue of Jacobian matrix for Poincaré return map.

II. RELATED WORKS

A. Rimless Wheel Model

This section outlines the discrete dynamics of a rimless wheel model shown in Fig. 2. This model consists of massless leg flames whose length is l [m] and the total mass, M [kg], is concentrated at the central position. The relative angle between the leg flames is α [rad].

Given a suitable initial condition, the rimless wheel rolls down a slope, and the rolling pattern converges to 1-period

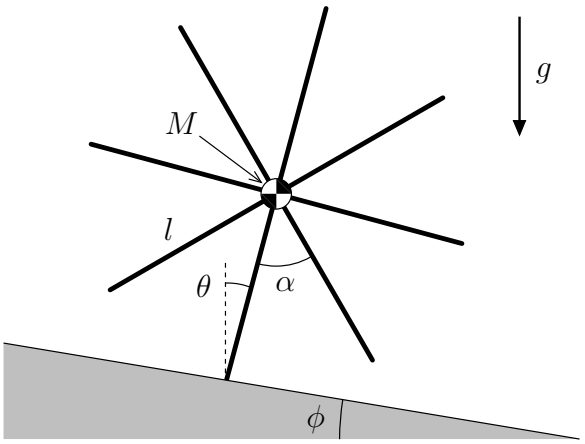

Fig. 2. Rimless wheel model.

stable limit cycle if the next collision always occurs. The stability principle is explained as follows.

Let i be the step number and K [J] be the kinetic energy. The kinetic energy just before impact satisfies the following simple recurrence formula:

$$K^-[i+1] = \varepsilon K^-[i] + \Delta E, \tag{1}$$

where $\varepsilon := K^+/K^- = \cos^2\alpha$ [-] is the energy-loss coefficient, $\Delta E = 2Mgl\sin\frac{\alpha}{2}\sin\phi$ [J] is the restored mechanical energy, and superscripts "+" and "−" respectively stand for immediately after and immediately before impact. Since both ε and ΔE are constant, Eq. (1) leads to

$$\lim_{i\to\infty} K^-[i] = \frac{\Delta E}{1-\varepsilon}, \tag{2}$$

which proves asymptotic stability.

Energy-loss coefficient specifies the convergence speed to the steady gait as well as the loss rate of the kinetic energy, so it should be constant to improve the limit cycle stability.

B. Simplest Walking Model

The simplest walking model, a compass-like biped model whose hip mass is sufficiently larger than the leg mass [6], also behaves in the same manner as a rimless wheel if the hip angle at impact is kept constant. Its discrete dynamics has been analyzed in detail by Ikemata *et al.* [10], and Wisse *et al.* also reported related results [9].

While their analysis approaches based on the Poincaré return map are complicated, the recurrence formula of Eq. (1) can clearly explain asymptotic stability of the generated gait. If the simplest walking model exhibits passive dynamic walking keeping the hip angle at impact constant, both ε and ΔE becomes constant simultaneously and their values are the same as the rimless wheel. This result strongly depends on the special property of the simplest walking model. The value of ε is determined only by the hip angle at impact regardless of the swing-leg's angular velocity just before impact in this model. In other words, SLR does not affect the impact dynamics of the simplest walking model.

In the following sections, we will analyze the energy-loss coefficient in general compass-like biped models whose leg mass cannot be neglected. Especially, the effects of SLR and mass-distribution are investigated.

III. COMPASS-LIKE BIPED ROBOT AND ITS ENERGY-LOSS COEFFICIENT

A. Dynamic Equation

Fig. 3 shows the model of a planar, fully-actuated, compass-like biped robot with flat feet. Two joint torques, u_1 and u_2, can be exerted at the ankle joint and hip joint. Let $\boldsymbol{\theta} = \begin{bmatrix}\theta_1 & \theta_2\end{bmatrix}^{\mathrm{T}}$ be the generalized coordinate vector, where θ_1 and θ_2 are the angular positions of the stance and swing legs with respect to vertical. The dynamic equation then becomes

$$\boldsymbol{M}(\boldsymbol{\theta})\ddot{\boldsymbol{\theta}} + \boldsymbol{C}(\boldsymbol{\theta},\dot{\boldsymbol{\theta}})\dot{\boldsymbol{\theta}} + \boldsymbol{g}(\boldsymbol{\theta}) = \boldsymbol{S}\boldsymbol{u} = \begin{bmatrix}1 & 1\\ 0 & -1\end{bmatrix}\begin{bmatrix}u_1\\ u_2\end{bmatrix}. \tag{3}$$

These matrices are described in detail elsewhere [2]. If we assume inelastic collisions for the stance-leg exchange and set suitable values for the physical parameters, the robot can exhibit passive dynamic walking on a gentle slope. Let E be the total mechanical energy of the robot, and relationship $\dot{E} = \dot{\boldsymbol{\theta}}^{\mathrm{T}}\boldsymbol{S}\boldsymbol{u}$ between the mechanical energy and the control inputs holds.

B. Transition Equation

The modeling of an inelastic collision is briefly described here. A more detailed explanation is given elsewhere [5]. We extended the configuration as shown in Fig. 4. We define the stance and swing legs immediately before impact as "Leg 1" and "Leg 2" and derive their dynamic models independently. We define $\boldsymbol{q}_i = \begin{bmatrix}x_i & z_i & \theta_i\end{bmatrix}^{\mathrm{T}}$ as the extended coordinate vector for Leg i and define $\boldsymbol{q} = \begin{bmatrix}\boldsymbol{q}_1^{\mathrm{T}} & \boldsymbol{q}_2^{\mathrm{T}}\end{bmatrix}^{\mathrm{T}}$ as that of the

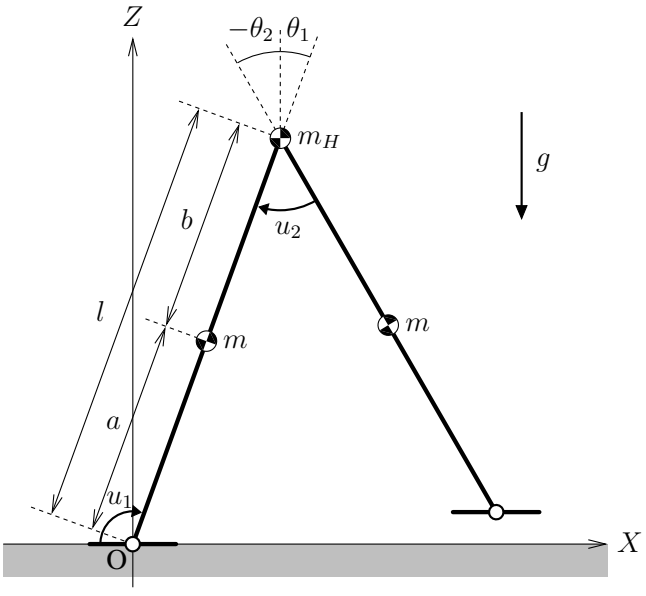

Fig. 3. Model of planar fully-actuated compass-like biped robot.

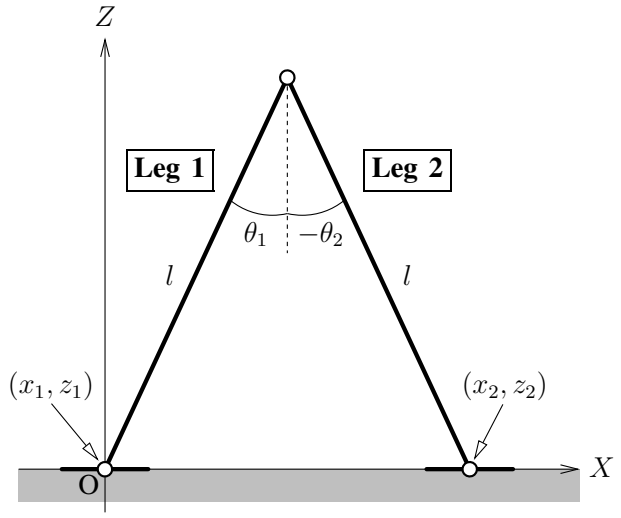

Fig. 4. Configuration at instant of heel strike.

whole system. The inelastic collision model is then derived as

$$\bar{\boldsymbol{M}}(\alpha)\dot{\boldsymbol{q}}^{+} = \bar{\boldsymbol{M}}(\alpha)\dot{\boldsymbol{q}}^{-} - \boldsymbol{J}_I(\alpha)^{\mathrm{T}}\boldsymbol{\lambda}_I, \tag{4}$$

where $\bar{\boldsymbol{M}} \in \mathbb{R}^{6\times 6}$ is the inertia matrix corresponding to $\boldsymbol{q}$ and α [rad] is the half inter-leg angle at impact and is defined as

$$\alpha := \frac{\theta_1^- - \theta_2^-}{2} = \frac{\theta_2^+ - \theta_1^+}{2} > 0. \tag{5}$$

Matrices $\bar{\boldsymbol{M}}$ and $\boldsymbol{J}_I$ are functions of α. The $\boldsymbol{J}_I \in \mathbb{R}^{4\times 6}$ is the Jacobian matrix derived from the geometric constraint conditions at the instant of heel strike; it should satisfy the following velocity constraint condition at immediately after impact:

$$\boldsymbol{J}_I(\alpha)\dot{\boldsymbol{q}}^{+} = \boldsymbol{0}_{4\times 1}. \tag{6}$$

The detailed derivations of matrix $\boldsymbol{J}_I(\alpha)$ and $\boldsymbol{\lambda}_I \in \mathbb{R}^4$ as the Lagrange undetermined multiplier vector representing the impact force are described elsewhere [5].

Following Eqs. (4) and (6), we can derive the velocity vector just after impact as

$$\dot{\boldsymbol{q}}^{+} = \boldsymbol{Y}(\alpha)\dot{\boldsymbol{q}}^{-}, \tag{7}$$

where

$$\boldsymbol{Y}(\alpha) = \boldsymbol{I}_6 - \bar{\boldsymbol{M}}^{-1}\boldsymbol{J}_I^{\mathrm{T}}\left(\boldsymbol{J}_I\bar{\boldsymbol{M}}^{-1}\boldsymbol{J}_I^{\mathrm{T}}\right)^{-1}\boldsymbol{J}_I, \tag{8}$$

We further obtain

$$\dot{\boldsymbol{\theta}}^{+} = \begin{bmatrix} 0&0&0&0&0&1 \\ 0&0&1&0&0&0 \end{bmatrix}\boldsymbol{Y}(\alpha)\boldsymbol{H}(\alpha)\dot{\boldsymbol{\theta}}^{-} =: \boldsymbol{\Xi}(\alpha)\dot{\boldsymbol{\theta}}^{-}, \tag{9}$$

where $\boldsymbol{H} = \boldsymbol{H}(\alpha) \in \mathbb{R}^{6\times 2}$ is the transfer matrix from $\dot{\boldsymbol{\theta}}^{-}$ to $\dot{\boldsymbol{q}}^{-}$ and is detailed as

$$\boldsymbol{H}(\alpha) = \begin{bmatrix} 0 & 0 \\ 0 & 0 \\ 1 & 0 \\ l\cos\alpha & -l\cos\alpha \\ -l\sin\alpha & -l\sin\alpha \\ 0 & 1 \end{bmatrix}. \tag{10}$$

C. Energy-loss Coefficient

By using Eq. (9), the kinetic energies just after and just before impact can be written as

$$K^{+} = \frac{1}{2}\left(\dot{\boldsymbol{\theta}}^{-}\right)^{\mathrm{T}}\boldsymbol{\Xi}(\alpha)^{\mathrm{T}}\boldsymbol{M}(\alpha)\boldsymbol{\Xi}(\alpha)\dot{\boldsymbol{\theta}}^{-}, \tag{11}$$

$$K^{-} = \frac{1}{2}\left(\dot{\boldsymbol{\theta}}^{-}\right)^{\mathrm{T}}\boldsymbol{M}(\alpha)\dot{\boldsymbol{\theta}}^{-}. \tag{12}$$

By using these equations, we can define the energy-loss coefficient as $\varepsilon := K^{+}/K^{-}$. This is a dimension-less quantity, and we can find $0 < \varepsilon < 1$ because $0 < K^{+} < K^{-}$.

Fig. 5 shows the 3D plot of ε with respect to $\dot{\theta}_1^-$ and $\dot{\theta}_2^-$ where the physical parameters of the compass-like biped model are chosen as in Table I. Fig. 6 shows the contour of the 3D plot on $\dot{\theta}_1^-$-$\dot{\theta}_2^-$ plane. The dotted (45°) line indicates ZSLR, i.e., $\dot{\theta}_1^- = \dot{\theta}_2^-$. In the area above this line $\left(\dot{\theta}_1^- < \dot{\theta}_2^-\right)$, ε fluctuates wildly. We can see that all contours seem to be straight lines which intersect the origin. This is true and we mathematically show it in the next section. Whereas in the area of $\dot{\theta}_1^- > \dot{\theta}_2^-$, ε is kept almost constant because there are no contours.

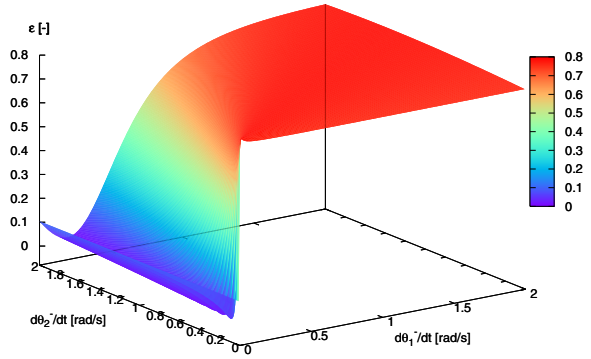

Fig. 5. 3D plot of ε with respect to $\dot{\theta}_1^-$ and $\dot{\theta}_2^-$. The physical parameters of the biped model are chosen as Table I.

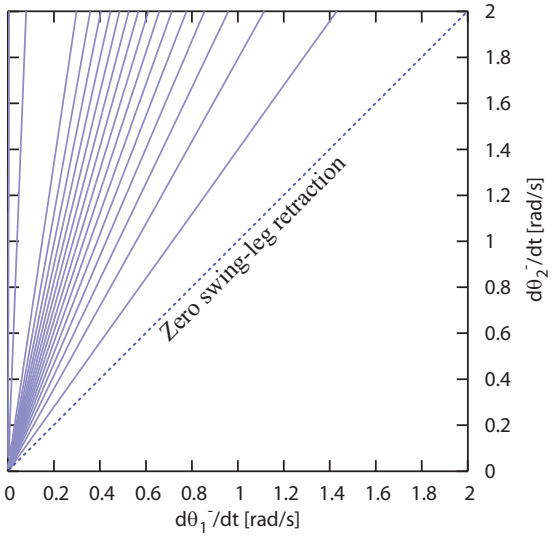

Fig. 6. Contours of 3D plot of ε with respect to $\dot{\theta}_1^-$ and $\dot{\theta}_2^-$.

TABLE I

PHYSICAL PARAMETERS OF COMPASS-LIKE BIPED MODEL

a	0.5	m
b	0.5	m
$l\ (=a+b)$	1.0	m
m_H	10.0	kg
m	5.0	kg
α	0.20	rad

IV. ANALYSIS RESULTS

A. General Formulation

We generalize the energy-loss coefficient taking SLR into account. Let ν [-] be the ratio of angular velocity just before impact which satisfies the following relation:

$$\dot{\theta}_2^- = \nu \dot{\theta}_1^-. \tag{13}$$

The angular velocities just after impact in Eq. (9) can then be rewritten as

$$\dot{\boldsymbol{\theta}}^+ = \boldsymbol{\Xi}(\alpha) \begin{bmatrix} 1 \\ \nu \end{bmatrix} \dot{\theta}_1^-. \tag{14}$$

Using this relation, we can rearrange the kinetic energies in Eqs. (11) and (12) as

$$\begin{aligned} K^+ &= \frac{1}{2} \begin{bmatrix} 1 \\ \nu \end{bmatrix}^{\mathrm{T}} \boldsymbol{\Xi}(\alpha)^{\mathrm{T}} \boldsymbol{M}(\alpha) \boldsymbol{\Xi}(\alpha) \begin{bmatrix} 1 \\ \nu \end{bmatrix} \left(\dot{\theta}_1^-\right)^2 \\ &=: \frac{1}{2} \hat{M}^+ \left(\dot{\theta}_1^-\right)^2, \end{aligned} \tag{15}$$

$$\begin{aligned} K^- &= \frac{1}{2} \begin{bmatrix} 1 \\ \nu \end{bmatrix}^{\mathrm{T}} \boldsymbol{M}(\alpha) \begin{bmatrix} 1 \\ \nu \end{bmatrix} \left(\dot{\theta}_1^-\right)^2 \\ &=: \frac{1}{2} \hat{M}^- \left(\dot{\theta}_1^-\right)^2. \end{aligned} \tag{16}$$

Using these equations, we can simplify the energy loss coefficient as

$$\varepsilon := \frac{K^+}{K^-} = \frac{\hat{M}^+}{\hat{M}^-}. \tag{17}$$

Here, define the following dimension-less parameters:

$$\beta := \frac{a}{l}, \tag{18}$$

$$\gamma := \frac{m_H}{m}. \tag{19}$$

The scalar functions $\hat{M}^+$ and $\hat{M}^-$ are then written as functions of α, β, γ and ν. They are detailed as follows.

$$\begin{aligned} \hat{M}^+(\alpha,\beta,\gamma,\nu) := {} & \frac{ml^2}{1+2\beta^2+2\gamma-\cos(4\alpha)} \\ & \times \left(2\beta^2+2\beta^4+2\beta\gamma+2\beta^2\gamma+\gamma^2\right. \\ & +2\beta^2\nu^2(1-\beta)^2+\gamma(2\beta+\gamma)\cos(4\alpha) \\ & \left.-4\beta\nu(1-\beta)(\beta+\gamma)\cos(2\alpha)\right) \end{aligned} \tag{20}$$

$$\begin{aligned} \hat{M}^-(\alpha,\beta,\gamma,\nu) := {} & ml^2\left(1+\beta^2+\gamma+(1-\beta)^2\nu^2\right. \\ & \left.-2\nu(1-\beta)\cos(2\alpha)\right) \end{aligned} \tag{21}$$

In the following, we treat ε as a function of the four parameters.

Fig. 7 plots ε with respect to ν for six values of γ where $\alpha = 0.20$ [rad] and $\beta = 0.50$ [-]. Note that the value of γ in the previous section was 2.0. We can see that, as ν rises above 1.0, the values of ε begin to decrease and converges to constant values. Wisse *et al.* mentioned that gentle SLR improves the gait stability [8][9]. This is true in the sense that the convergence speed becomes high or ε becomes small when ν is larger than 1.0, i.e., SLR occurs. In the following, we mathematically analyze this result in more detail.

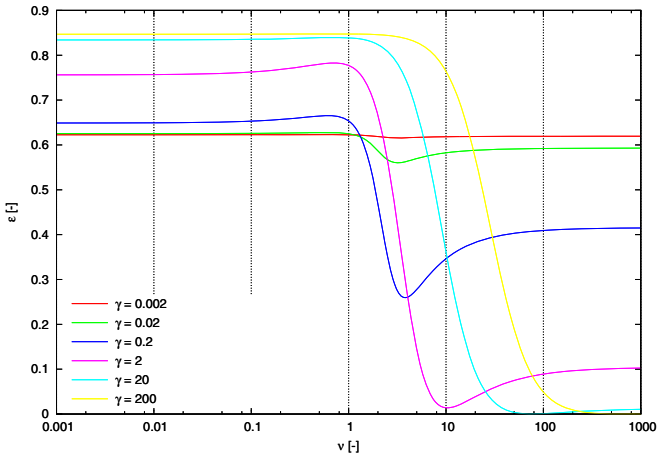

Fig. 7. ν versus ε for six values of γ where $\alpha = 0.20$ [rad] and $\beta = 0.50$ [-].

B. Effect of γ on ε

We first discuss the effect of mass-distribution. ε is a scalar function of the four parameters, however, there are two special cases:

$$\lim_{\gamma\to\infty} \varepsilon(\alpha,\beta,\gamma,\nu) = \cos^2(2\alpha), \tag{22}$$

$$\lim_{\gamma\to+0} \varepsilon(\alpha,\beta,\gamma,\nu) = \frac{2\beta^2}{1+2\beta^2-\cos(4\alpha)}. \tag{23}$$

These do not depend on ν. The upper case is for the simplest walking model [5]. In these cases, the motion of the swing leg just before impact does not affect the energy loss at all, and all we have to do to keep ε constant is to keep α constant. In this sense, we can conclude that mass-distribution disturbs the energy-loss property which affects the gait stability. Such conditions of robot's mass distribution are, however, unrealistic or physically impossible.

In addition, from Eq. (23), we can find that the robot completely loses the kinetic energy when $\beta = 0$, and the walking motion then stops. Whereas we can find that the robot also stops when $2\alpha = \pi/2$ from Eq. (22); the simplest walking model must avoid this condition to continue walking.

Fig. 8 shows the closeup of Fig. 7 where $0.001 \le \nu \le 4$. This range of value is proper for general limit cycle walking. The values of ε where $\gamma = 0$ and ∞ are also indicated in the figure.

It is sure that the following inequality holds if $\nu \le 1.0$ (See the colored domain in Fig. 8).

$$\frac{2\beta^2}{1+2\beta^2-\cos(4\alpha)} \le \varepsilon(\alpha,\beta,\gamma,\nu) \le \cos^2(2\alpha) \tag{24}$$

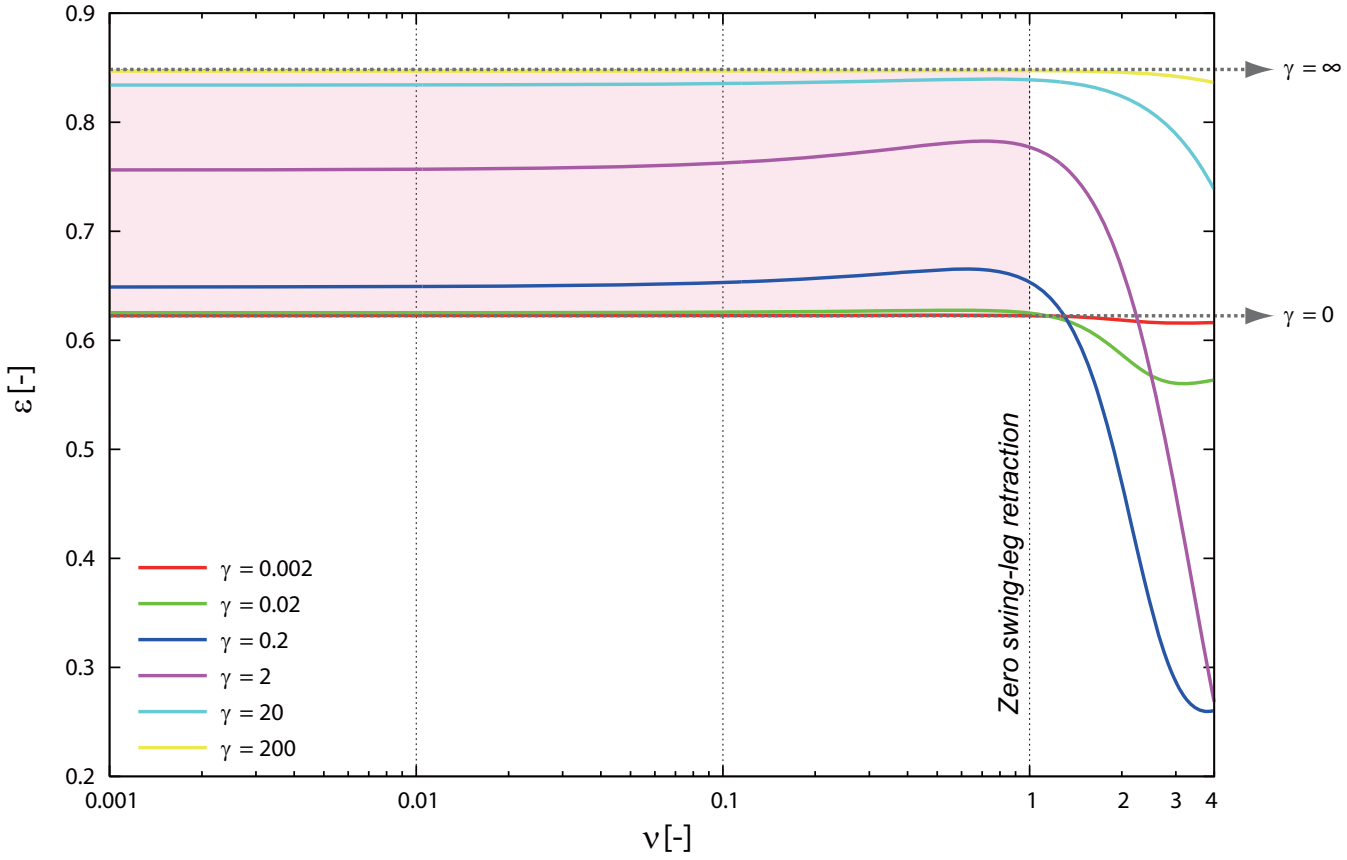

Fig. 8. Closeup of Fig. 7 where $0.001 \leq \nu \leq 4$. Two values of ε where $\gamma = 0$ and ∞ are also indicated.

C. *Effect of ν on ε*

Next, we discuss the effect of SLR. As mentioned, ε converges to a constant as $\nu \to +0$ or $\nu \to \infty$. This is analytically proved as follows.

$$\lim_{\nu \to \infty} \varepsilon\left(\alpha, \beta, \gamma, \nu\right) = \frac{2\beta^2}{1 + 2\beta^2 + 2\gamma - \cos(4\alpha)} \tag{25}$$

$$\lim_{\nu \to +0} \varepsilon\left(\alpha, \beta, \gamma, \nu\right) = \frac{2(\beta + \gamma)^2}{1 + 2\beta^2 + 2\gamma - \cos(4\alpha)} - \frac{\gamma(2\beta + \gamma)}{1 + \beta^2 + \gamma} \tag{26}$$

We further obtain the following limit values.

$$\lim_{\gamma \to +0} \left(\lim_{\nu \to \infty} \varepsilon\left(\alpha, \beta, \gamma, \nu\right) \right) = \frac{2\beta^2}{1 + 2\beta^2 - \cos(4\alpha)} \tag{27}$$

$$\lim_{\gamma \to +0} \left(\lim_{\nu \to +0} \varepsilon\left(\alpha, \beta, \gamma, \nu\right) \right) = \frac{2\beta^2}{1 + 2\beta^2 - \cos(4\alpha)} \tag{28}$$

These values are equal to Eq. (23). This result supports that the curve of ε where $\gamma = 0.002$ in Fig. 7 is very close to the constant value where $\gamma = 0$. On the other hand, the curve of ε where $\gamma = 200$ converges to the limit value of Eq. (22) as $\nu \to +0$, as shown in Fig. 8. Whereas it converges to 0 as $\nu \to \infty$. This can be easily understood from Eq. (25) as

$$\lim_{\gamma \to \infty} \left(\lim_{\nu \to \infty} \varepsilon\left(\alpha, \beta, \gamma, \nu\right) \right) = 0. \tag{29}$$

It is obvious that the kinetic energy loss becomes large or ε becomes smaller when the robot slams the swing leg wildly on the floor. The plot of Fig. 7 shows that, however, there exists a local minimal value in each curve of ε. In addition, note that the limit value of Eq. (29) is different from that of Eq. (22), that is, the limits for ν and for γ cannot be exchanged. We leave the detailed discussion for another opportunity.

The important result is that ε is settled in the range of $\nu \leq 1.0$. In this case, the swing leg (relative hip angle) extends just prior to impact. By achieving this and keeping the hip angle at impact simultaneously, we can improve the limit cycle stability and energy-efficiency because ε is maintained virtually constant and is kept large.

V. DISCUSSION

Ikemata *et al.* derived the eigenvalues of Jacobian matrix for Poincaré return map, $\boldsymbol{J}_f \in \mathbb{R}^{2\times 2}$, by utilizing the property of the simplest walking model. Matrix $\boldsymbol{J}_f$ has two eigenvalues: 0 and $\cos^2(2\alpha)$. The physical meaning of these values, however, has not been clarified. This section discusses the relation between the energy-loss coefficient and the above eigenvalues.

If the four parameters, α, β, γ and ν, are constant, then ε becomes constant. In the case of passive dynamic walking, ΔE also becomes constant. The discrete behavior of the walking system satisfies the recurrence formula of Eq. (1).

Let $\dot{\theta}_*^-$ [rad/s] be the steady value of $\dot{\theta}_1^-$, then Eq. (1) can be rewritten as

$$\frac{\hat{M}^-}{2}\left(\dot{\theta}_1^-[i+1]\right)^2 = \varepsilon\frac{\hat{M}^-}{2}\left(\dot{\theta}_1^-[i]\right)^2 + \Delta E. \quad (30)$$

The steady condition can also be rewritten as

$$\frac{\hat{M}^-}{2}\left(\dot{\theta}_*^-\right)^2 = \varepsilon\frac{\hat{M}^-}{2}\left(\dot{\theta}_*^-\right)^2 + \Delta E. \quad (31)$$

By using the relation

$$\dot{\theta}_1^-[i] = \dot{\theta}_*^- + \delta\dot{\theta}_1^-[i] \quad (32)$$

and the approximation

$$(x+\delta x)^2 \approx x^2 + 2\delta x, \quad (33)$$

the left hand side of Eq. (30) can be arranged as

$$\frac{\hat{M}^-}{2}\left(\dot{\theta}_*^- + \delta\dot{\theta}_1^-[i+1]\right)^2 \approx \frac{\hat{M}^-}{2}\left(\left(\dot{\theta}_*^-\right)^2 + 2\delta\dot{\theta}_1^-[i+1]\right), \quad (34)$$

whereas the right hand side of Eq. (30) is also arranged as

$$\begin{aligned} &\varepsilon\frac{\hat{M}^-}{2}\left(\dot{\theta}_*^- + \delta\dot{\theta}_1^-[i]\right)^2 + \Delta E \\ \approx\ &\varepsilon\frac{\hat{M}^-}{2}\left(\left(\dot{\theta}_*^-\right)^2 + 2\delta\dot{\theta}_1^-[i]\right) + \Delta E. \end{aligned} \quad (35)$$

Following Eqs. (30), (31), (34) and (35), we obtain

$$\delta\dot{\theta}_1^-[i+1] = \varepsilon\delta\dot{\theta}_1^-[i], \quad (36)$$

and this gives the proof that one of the eigenvalues not equal to 0 is ε, and the limit cycle is asymptotically stable. Note that ε is also equal to the maximum singular value.

VI. CONCLUSION AND FUTURE WORK

In this paper, we discussed the effects of SLR and mass-distribution on limit cycle walking from the energy-loss coefficient view-point. It is important that the condition $\dot{\theta}_1^- \geq \dot{\theta}_2^-$ ($\nu \leq 1.0$) achieves settling the energy-loss coefficient with large value. We also discussed the relation between the energy-loss coefficient and eigenvalue of the Poincaré return map. We conclude that the physical meaning of the eigenvalue is irrefutably-linked to the energy-loss.

In the future, we should investigate the validity of the derived results through analysis of dynamic bipedal walkers. The inequality of Eq. (24) should also be rigorously-proved.

REFERENCES

[1] T. McGeer, "Passive dynamic walking," *Int. J. of Robotics Research*, Vol. 9, No. 2, pp. 62–82, 1990.

[2] F. Asano, Z.W. Luo and M. Yamakita, "Biped gait generation and control based on a unified property of passive dynamic walking," *IEEE Trans. on Robotics*, Vol. 21, No. 4, pp. 754–762, 2005.

[3] F. Asano and Z.W. Luo, "Energy-efficient and high-speed dynamic biped locomotion based on principle of parametric excitation," *IEEE Trans. on Robotics*, Vol. 24, No. 6, pp. 754–762, 2008.

[4] A. Seyfarth, H. Geyer and H. Herr, "Swing-leg retraction: a simple control model for stable running," *J. of Experimental Biology*, Vol. 206, pp. 2547–2555, 2003.

[5] F. Asano and Z.W. Luo, "Asymptotically stable biped gait generation based on stability principle of rimless wheel," *Robotica*, 2009. (In press)

[6] M. Garcia, A. Chatterjee, A. Ruina and M. Coleman, "The simplest walking model: Stability, complexity, and scaling," *ASME J. of Biomechanical Engineering*, Vol. 120, No. 2, pp. 281–288, 1998.

[7] F. Asano and Z.W. Luo, "Robust pseudo virtual passive dynamic walking considering swing-leg retraction," *Proc. of the 26th Annual Conf. of the Robotics Society of Japan*, 3B1-05, 2008. (In Japanese)

[8] D. G. E. Hobbelen and M. Wisse, "Swing-leg retraction for limit cycle walkers improves disturbance rejection," *IEEE Trans. on Robotics*, Vol. 24, No. 2, pp. 377–389, 2008.

[9] M. Wisse, C. G. Atkeson and D. K. Kloimwieder, "Swing leg retraction helps biped walking stability," *Proc. of the IEEE-RAS Int. Conf. on Humanoid Robots*, pp.295–300, 2005.

[10] Y. Ikemata, A. Sano and H. Fujimoto, "A stability mechanism of the fixed point in passive walking," *J. of the Robotics Society of Japan*, Vol. 23, No. 7, pp. 839–846, 2005. (In Japanese)